JJMIE

Volume 18, Number 2, June. 2024
ISSN 1995-6665
Pages 267- 285
https://doi.org/10.59038/jjmie/180202
Editor-in-Chief: Prof. Ali M. Jawarneh

Jordan Journal of Mechanical and Industrial Engineering

NH_3-H_2-Working Fluid-based Shell and Tube Heat Exchanger and the H_2O-to-H_2O Helical Heat Exchanger: A Novel Integration to Ammonia Production Plants

Anwar Hamdan Al Assaf[1], Abrar Ahmed[2], Dima Muawiya Mahaftha[2], Abdulkarem I. Amhamed[2,*], Odi Fawwaz Alrebei[2], Bilal A. Jarrah[1]

[1]Department of Aviation Sciences, Amman Arab University, Amman 11953, Jordan
[2]Qatar Environment and Energy Research Institute (QEERI), Hamad Bin Khalifa University, Doha 34110, Qatar

Received 23 Jan 2024 Accepted 6 Mar 2024

Abstract

This study assesses global efforts to enhance existing ammonia plants and explores the feasibility of integrating heat exchangers at different stages of ammonia production. Based on this, the researchers analyzed two heat exchange systems, namely the NH_3-H_2 shell and tube heat exchanger and the H_2O-to-H_2O helical heat exchanger, in order to investigate their objectives. This study investigated the use of different NH_3-H_2 compositions as working fluids in shell and tube heat exchangers, specifically focusing on the shell and tube heat exchanger. The ASPEN HYSYS software was utilized for this analysis. This investigation conducted a comprehensive analysis of different sensitivity analyses to assess the influence of ammonia efficiency on the cooling process. The utilization of shell and tube heat exchangers in cooling applications, specifically those with high ammonia concentrations, can result in a more compact design for the heat exchanger. The observed outcome can be explained by the advantageous characteristics of ammonia, such as its higher heat capacity and improved heat transport properties compared to water. Furthermore, the study utilized a computational fluid dynamics (CFD) approach, specifically employing ANSYS Fluent for the analysis. The helical design of the heat exchanger efficiently distributes heat flux under specific conditions. The heat flow decreases gradually along the length of the exchanger due to this distribution.

Keywords: Ammonia Production; Ammonia, heat recovery, CFD.

1. Introduction

1.1. The importance of ammonia (NH_3)

Ammonia (NH_3) is crucial in the industrial sector and is widely recognized as the most cost-effective source of combined nitrogen. The production of this substance involves the processing of raw materials and relies significantly on the use of products with approximately 76% nitrogen content, as depicted in Figure 1 [1]. Ammonia (NH_3) is synthesized through a highly energetic reaction between nitrogen gas (N_2) and hydrogen gas (H_2) under extreme temperature and pressure conditions, facilitated by a suitable catalyst. The product derived from this process is commonly referred to as synthetic ammonia. Ammonia (NH_3) is produced as a byproduct of coal combustion [2].

However, it is important to recognize that the aforementioned ammonia type, known as byproduct ammonia, yields considerably less than synthetic ammonia. The Haber-Bosch process is widely employed worldwide, albeit at significant cost. Mont C. [3] has made various enhancements to the Haber & Bosch method, including modifications to operational parameters, catalysts employed, and the generation and preservation of hydrogen and nitrogen. Atmospheric nitrogen is the primary source of nitrogen for ammonia synthesis, while natural gas obtained through steam-methane reforming serves as the primary source of hydrogen.

Another important consideration is the availability of conversion facilities in ammonia plants, as these facilities can produce both CH_3OH and NH_3 [4]. During periods of peace, NH_3 is primarily employed for the production of N_2-based fertilizer, HNO_3, and other diverse applications. Liquid ammonia is frequently employed as a refrigerant in commercial refrigeration due to its cost-effectiveness and superior thermal characteristics [5]. Liquefied ammonia has multiple applications, such as serving as a cost-effective alkali, improving the rigidity of steel-based materials [6], and aiding in water purification [7]. Synthetic ammonia is crucial in warfare due to its essential role in the production of all non-nuclear military explosives. The expansion of the ammonia sector is crucial for ensuring national security in light of the growing influence of new ideologies and philosophies globally.

* Corresponding author e-mail: aamhamed@hbku.edu.qa.

1.2. Modern ammonia production plants

Modern NH_3 production facilities use the steam-methane-reforming (SMR) technique to produce anhydrous ammonia. The process involves the introduction of H_2, which reacts with N_2 under high temperature and pressure conditions with the aid of a catalyst. The compound is synthesized under conditions of 20 MPa pressure and 730 K temperature. Figure 2 [8, 9] illustrates the steps involved in the SMR process. The term "Haber-Bosch (HB) process" is used to refer to this stage. The production of ammonia requires the use of fossil fuels and the availability of air and water as necessary inputs. Natural gas is the primary fossil fuel source, accounting for approximately 76% of global NH_3 production. Coal-fired power stations account for approximately 24% of the total capacity within the energy sector.

To enhance the efficiency of the steam methane reforming (SMR) process, a small quantity of hydrogen gas (H_2) is introduced into natural gas and subsequently heated to approximately 730 K. The preheating process can be conducted either within the integrated reforming furnace or through the utilization of external heat sources such as heat exchangers or heaters.

To prevent potential poisoning of the nickel-based catalyst in the second reactor, it is essential to reduce the molar fraction of sulfur-based contents (H_2S and organic S compounds) in the preheated gas mixture to below 1%. This can be accomplished by arranging one or two reactors in a sequential manner. The initial reactor utilizes a cobalt molybdenum (Co-Mo) catalyst, whereas the subsequent reactor necessitates a zinc oxide (ZnO) adsorbent. Dividing the reformer unit into two stages is a viable approach. The primary reformer is a key component of a methane reforming facility. It is responsible for introducing a mixture of steam and methane, with a molar ratio of 1:4. The mixture is heated by radiation as it flows through channels containing a nickel-based reforming catalyst.

As a result, methane undergoes partial conversion, resulting in the formation of hydrogen (H_2), carbon monoxide (CO), and carbon dioxide (CO_2). On average, this conversion process represents around 66% of the initial methane supply [10]. The initial reformer utilizes gas-fueled burners to generate heat. The burners can be categorized as side-fired, top-fired, or bottom-fired. A convection bank is used to recycle the heat produced in the boiler enclosure, specifically the thermal energy from the flue gas, for other purposes such as supercritical steam heating and preheating process air.

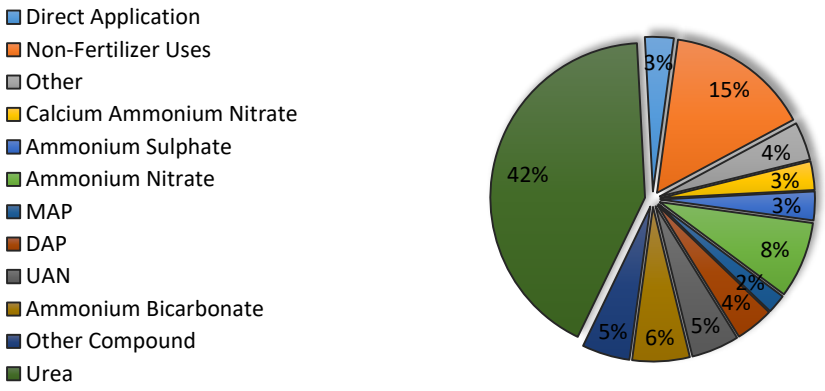

Figure 1. The applications of ammonia (NH3).

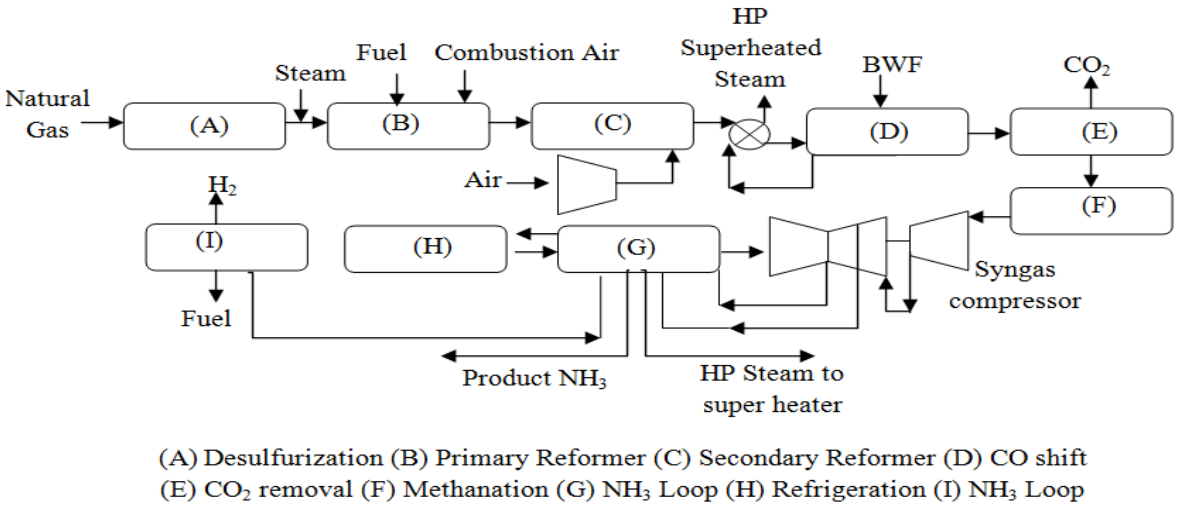

Figure 2. Block diagram of conventional NH3 production.

Thus, as previously mentioned, ammonia production plants must employ innovative techniques to reduce energy consumption. This paper focuses on researching the integration of heat recovery measures as one of the techniques to make the cycle more efficient by considering essential premetallized below.

- Heat flow at the cold stream inlet vs. the temperature of the hot stream outlet
- Heat flow at the cold stream inlet vs. the pressure of the hot stream outlet
- Heat flow at the cold stream inlet vs. the pressure of the cold stream outlet
- Cold stream inlet temperature vs LMTD of the heat exchanger

Figure 2 demonstrates the potential for heat exchanger implementation. However, additional heat exchangers could be employed in alternative configurations of ammonia plants. Figure 3 depicts the KBR design of a single-train ammonia plant, which incorporates a substantial number of heat exchanges (approximately 18 locations throughout the plant). H_2O-to-H_2O heat exchangers are utilized in these locations. This study examines the feasibility of using a helical heat exchanger for H_2O-to-H_2O applications. The performance of the heat exchanger is evaluated through a computational fluid dynamics (CFD) analysis using ANSYS-Fluent.

2. Methodology

The methodology was divided into two sections. The first section provided a detailed explanation of the helical heat exchanger, including its main geometry and specific conditions for different models. The following section discusses the design of a shell and tube heat exchanger using the ASPEN HYSYS software platform.

2.1. Helical heat exchanger

Heat transfer in helical coil heat exchangers involves the exchange of thermal energy between fluids traversing a helically coiled conduit. This configuration is advantageous due to its compactness, heightened heat transfer rates, and adaptability across diverse applications. The helical coil's geometry induces fluid turbulence, fostering increased heat transfer efficiency by augmenting convective heat transfer coefficients and reducing thermal boundary layers. This turbulence facilitates greater interaction between the fluid and the tube wall, amplifying the heat transfer process. Furthermore, the helical coil's design expands the available surface area for heat exchange within a confined volume, rendering it proficient in transferring heat between fluids with substantial temperature differentials. Its spatial efficiency makes helical coil heat exchangers particularly suitable for environments where space constraints are pertinent.

Developing an experimental prototype is essential in the initial phase of adjusting or proposing a new heat exchanger for ammonia plants. A CFD model of the heat exchanger in the ammonia plant prototype was developed using ANSYS Fluent. The heat exchanger design includes a copper H_2O-to-H_2O shell and coiled tube, following the dimensions described in Table 1. This model was created to predict the performance of the heat exchanger before manufacturing the experimental setup. Figure 4 illustrates the CFD model [15, 23].

Table 1. The dimensional parameters of the shell and coiled tube heat exchanger.

Parameter	Value [mm]
Number of coils	10
Tube thickness	0.157
L	225
D	120
S	10
d1	12
d2	16
b	21.4

Table 2 describes the model's boundary conditions, including the temperature, pressure, and velocity conditions of the inlet and the outlet streams and the materials used in the model.

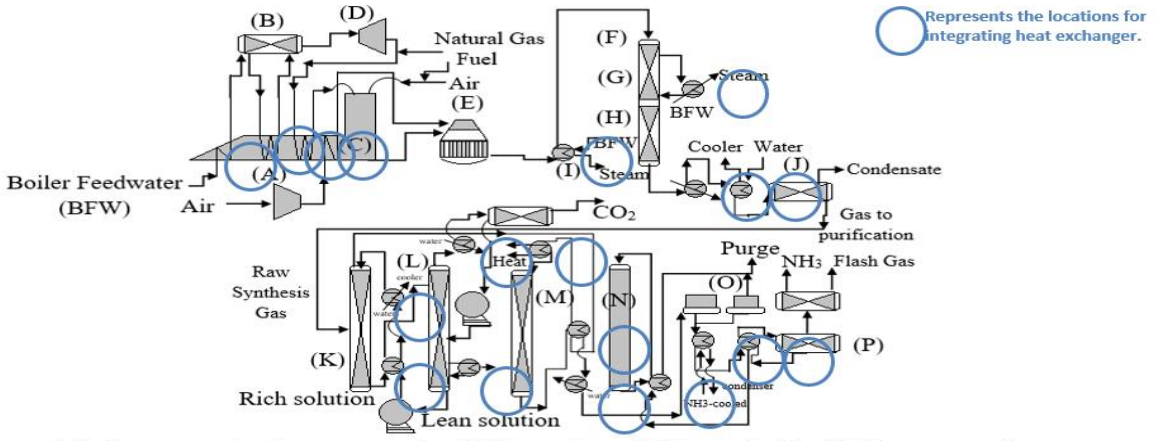

(A) Compressor, heat recovery section (B) Steam Drum (D) Power turbine (E) Secondary reformer (F) CO convertor (G) First stage high-temperature synthesis (H) Second stage low-temperature Synthesis (I) BFW Heat recovery (J) Condensation (K) CO_2 absorber (L) CO_2 stripper (M) Methanator (N) NH_3 convertor (O) Compression (P) Separator

Figure 3. KBR design of the first single-train (large-capacity ammonia plant).

Table 2. The boundary conditions and material used in the heat exchanger.

Stream	Type of boundary condition	Corresponding condition
Cold Stream Inlet	Mass-flow-defined condition	Mass flow rate: 0.019 [L/s] Temperature: 10.9 [°C] Material: H_2O
Hot Stream Inlet	Mass-flow-defined condition	Mass flow rate: 0.0169 [L/s] Temperature: 33.4 [°C] Material: H_2O
Cold Stream Outlet	Pressure-defined condition	Pressure: 1 [bar]
Hot Stream Outlet	Pressure-defined condition	Pressure: 1 [bar]
Surrounding condition	Pressure-Temperature defined condition	Pressure: 1 [bar] Temperature: 27 [°C]

To simulate the performance of the heat exchanger, which is described in Figure 4, Tables 1 and 2, ANSYS Fluent has been utilized to obtain the overall heat transfer coefficient (U_o), by applying the following equations (1) and (2) [11].

$$twoLMTD = \frac{(\Delta T_2 - \Delta T_1)}{\ln(\Delta T_2/\Delta T_1)} \quad (1)$$

$$U_o = \frac{\dot{Q}}{A_o LMTD} \quad (2)$$

2.1.1. Methods of Data Analysis

The CFD simulation was conducted using the ANSYS Fluent 2021software on a virtual machine equipped with an Intel® Core™i7-7700 CPU running at 3.6 Hz. The virtual machine had 32 GB of installed memory and operated on a 64-bit operating system. The computational time for each case study was approximately 12 hours. The geometry was modeled and imported into ANSYS software to create the mesh for the heat exchanger model, as depicted in Figures 5a and 5b. The mesh quality metrics are displayed in Figure 6.

The Turbulence Kinetic Energy (k) is used to define the flow mixing level as per Equations (3-6) [12-14].

$$k = \frac{3}{2}(UI)^2 \quad (3)$$

$$\varepsilon = c_\mu^{\frac{3}{4}} k^{\frac{3}{2}} l^{-1} \quad (4)$$

$$I = 0.16 Re^{-\frac{1}{8}} \quad (5)$$

$$l = 0.07L \quad (6)$$

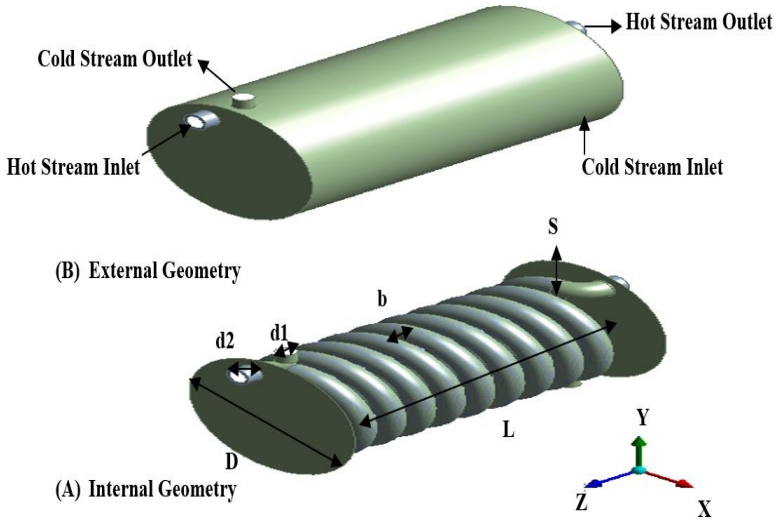

Figure 4. The shell and coiled tube for the helical heat exchanger model.

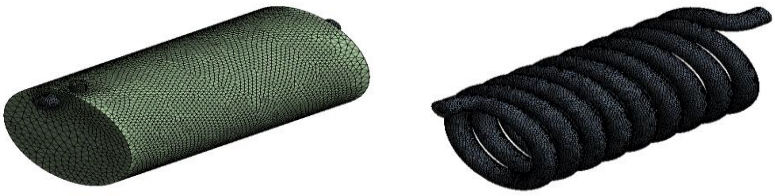

(a) **(b)**

Figure 5. The mesh of the helical heat exchanger model (external (**a**) and internal geometry (**b**)).

An Aspen HYSYS simulation was utilized to design a shell and tube heat exchanger for the purpose of cooling nitrogen and hydrogen gas mixture (hot stream) against water and ammonia (cold stream) in an ammonia production process [16, 28-30]. The heat exchanger design in Figure 7 was carefully implemented to enhance the cooling efficiency of the incoming gases, enabling them to achieve the desired temperatures for subsequent chemical reactions. The design parameters, such as heat exchanger type, dimensions, and heat transfer coefficients, were meticulously chosen to ensure effective heat exchange while maintaining compliance with safety and operational regulations [17, 22]. The heat exchanger is essential for efficient ammonia production, as it helps maintain optimal reaction conditions and enhances overall process efficiency [18, 24].

The designed heat exchanger was evaluated, and its thermal duty was determined to be $\mathbf{6.374 \times 10^{5} kJ/hr}$, with an overall heat transfer coefficient of $\mathbf{6.384 \times 10^{3} kJ/°C\,hr}$. The Logarithmic Mean Temperature Difference (LMTD) for the heat exchanger was calculated to be 99.83°C. The analysis revealed a hot pinch temperature of 90°C and a cold pinch temperature of 30°C. These parameters collectively demonstrate the heat exchanger's capacity to efficiently transfer heat between the hot and cold streams[19, 25], ensuring effective temperature control in the ammonia production process [20, 26].

As recommended by [21, 27], a sensitivity analysis was performed by altering the composition of the cold stream (water and ammonia) to study its effect on the following relations.

- Heat flow at the cold stream inlet vs. the temperature of the hot stream outlet
- Heat flow at the cold stream inlet vs. the pressure of the hot stream outlet
- Heat flow at the cold stream inlet vs. the pressure of the cold stream outlet
- Cold stream inlet temperature vs LMTD of the heat exchanger

The initial conditions for the designed heat exchanger are summarized in Table 3; these parameters are considered as the base case for the study.

3. Results

3.1. CFD analysis for helical heat exchanger

The provided CFD analyses in this paper aim to provide initial predication of an existing helical heat exchanger to be further analyzed experimentally. The CFD analysis of a water-to-water shell and coiled heat exchanger demonstrates a progressive reduction in heat flux along its length. Figure 8 illustrates the flow of hot water through the inner tube, with a flow rate of 0.0169 kg/s. This hot water transfers thermal energy to the surrounding cold water in the outer tube, which has a flow rate of 0.019 kg/s.

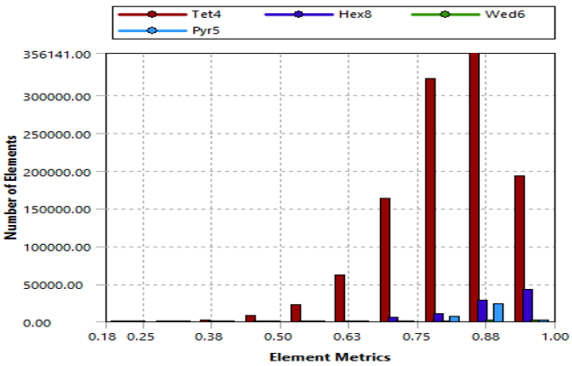

Figure 6. Mesh quality metrics.

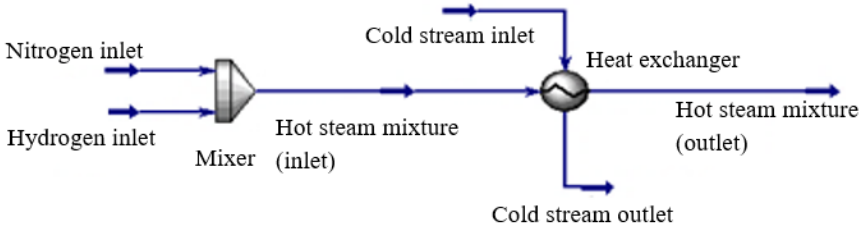

Figure 7. Shell and tube heat exchanger design.

Table 3. The initial conditions of the heat exchanger.

	Hot Stream				Cold Stream	
Stream	Hydrogen inlet	Nitrogen inlet	Mixed stream Inlet	Mixed stream outlet	water inlet	Water outlet
Vapor fraction	1	1	1	1	0	0
Temperature (C)	230	200	229.1	90	30	57
Pressure (kPa)	6640	6610	6610	6680	1013	1013
Mass flow (kg/h)	310	120	430	430	5468	5468
Heat flow (kJ/h)	9.118e+005	2.169e+004	9.335e+005	2.169e+005	-8.675e+007	-8.612e+007
Mass fraction	100% hydrogen	100% nitrogen	72% hydrogen and 28% nitrogen	72% hydrogen and 28% Nitrogen	100% water and 0% ammonia	100% water and 0% ammonia

Figure 9 displays the temperature contour, illustrating the thermal characteristics of the fluid within the tube and the temperature distribution across the heat exchanger. The contour is obtained from computational fluid dynamics (CFD) simulations, depicting a gradient from the inlet to the outlet. The hot water stream, initially at a temperature of 306.55 K, undergoes a gradual cooling process when it comes into contact with the cooler outer tube. The outer tube contains cold water entering at a temperature of 284.5 K. The cooling process results in a gradual decrease in temperature as the fluids continue to interact.

Temperature contouring was conducted along the length of the heat exchanger in various zones to observe the distribution of temperatures. Figure (9) displays the temperature range of 283 to 306 K at the inlet and outlet of the heat exchanger. The CFD analysis shows that the cooling process leads to a decrease in temperature gradient. This behavior can be attributed to the combined effects of heat conduction and convection.

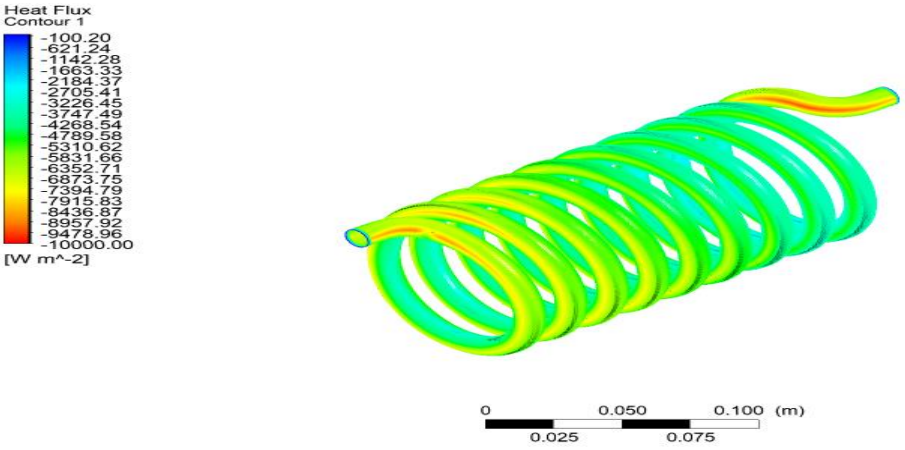

Figure 8. Heat flux contour along the length of heat exchanger model.

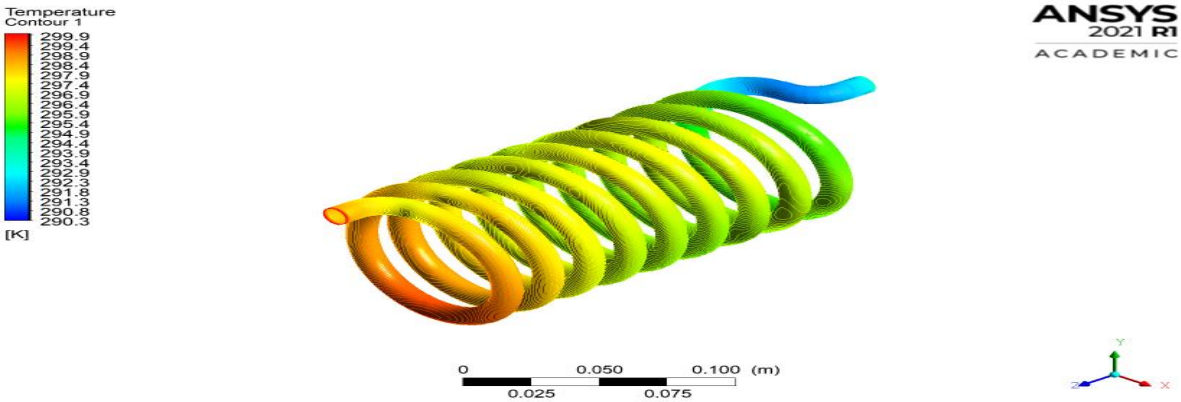

Figure 9. Temperature contour along the length of helical heat exchanger.

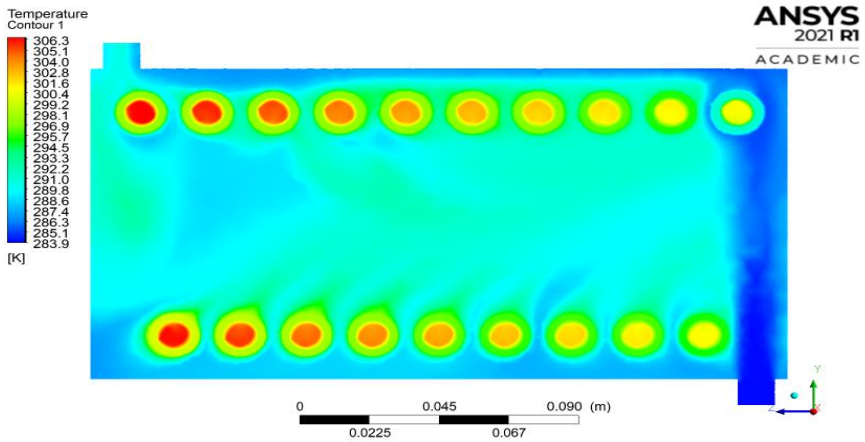

Figure 10. Temperature contour along the cut section the of heat exchanger model.

3.2. Heat exchanger sensitivity analysis (ASPEN)

The utilized numerical tool used in this paper (HTRI) does not provide alternative types of exchangers. However, it is used to provide comparable results with respect variable working fluids. By only altering the composition of the cooling fluid from pure water to a mixture of water and ammonia, it is possible to achieve lower heat flow rates and reduce the size of the heat exchanger. This outcome is attributed to the advantageous properties of ammonia, including its higher heat capacity and superior heat transfer characteristics compared to water, and it is represented in the following analyzed cases:

Case 1: As shown in Figure (11), The analysis resulted in four plots depending on different variables. In charts A, B, and D the data points have been analyzed using linear regression, resulting in a perfect fit for A and strong correlations for B and D, with R-squared values of 1, 0.9965, and 0.9871, respectively. In the case of chart C, a second-order polynomial regression has been applied, showing a rate of change of equation y'= -223630x + 14×10^7x ln (10). The R-squared value for chart C is 0.951, indicating a moderate relationship between water outlet temperature and heat exchanger (LMTD).

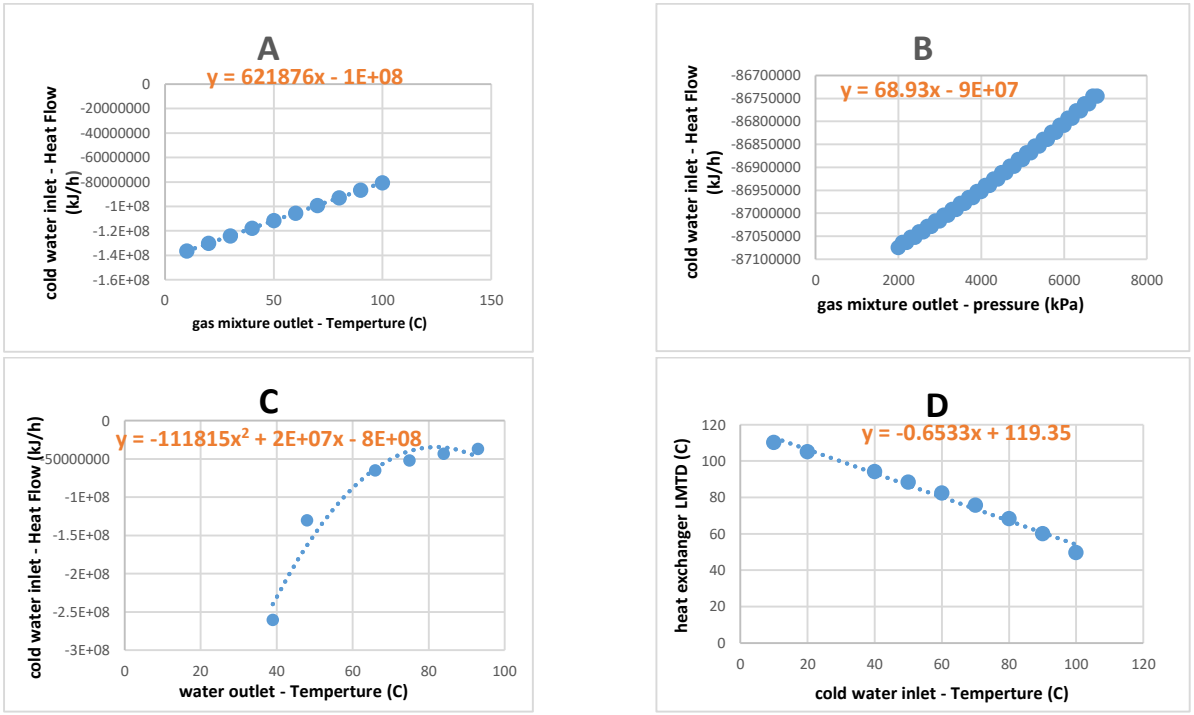

Figure 11: Sensitivity analysis cases at 100% H_2O and 0% NH_3 concentrations in different variables of interest combinations A, B, C, D (case1).

Table 4. Values of rate of change and coefficient of determination at 100% water,0% ammonia **(case1)**.

Variables of Interest	Rate of Change	R^2 Value
A	$= 621876$	$R^2 = 1$
B	$= 68.93$	$R^2 = 0.9965$
C	$= -223630x + 14 \times 10^{7x}\, ln(10)$	$R^2 = 0.951$
D	$= -0.6533$	$R^2 = 0.9871$

The rate of change was determined using the formula: $\frac{d}{dx}\,[x^n] = nx^{n-1}$

Case 2: The four plots Figure (12) at 90% water, 10% ammonia in charts A, B, and D with applying linear regression resulted in a straight line fit for chart for A and suitable correlations for B and D, with R-squared values of 1, 0.9961, and 0.951, respectively. A second-order polynomial regression was used for chart C revealing a rate of change described by y'= $-200918x + 14 \times 10^{7x}\, ln(10)$ The R-squared value for chart C stands at 0.951.

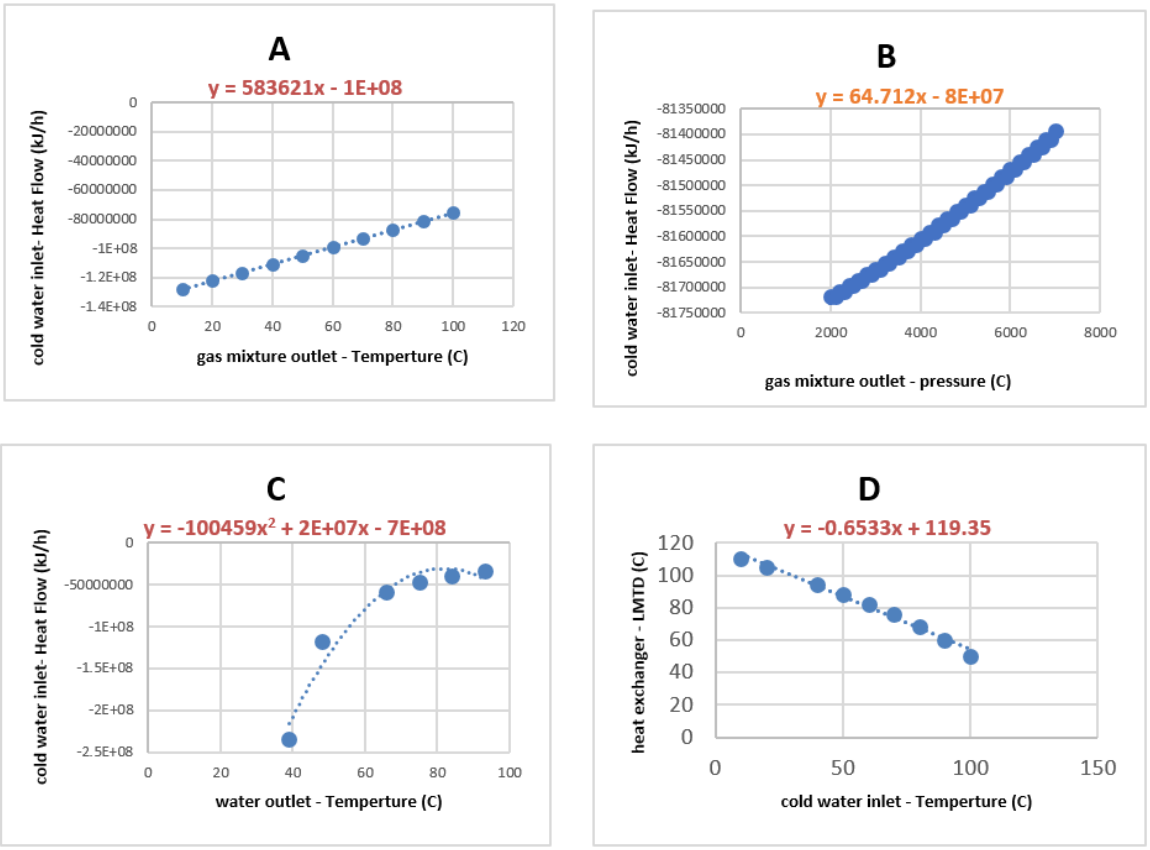

Figure 12: Sensitivity analysis cases at 90% H_2O and 10% NH_3 concentrations in different variables of interest combinations A, B, C, D (case2).

Table 5. Values of rate of change and coefficient of determination at 90% water,10% ammonia **(case2)**.

Variables of Interest	Rate of Change	R^2 Value
A	$= 583621$	$R^2 = 1$
B	$= 64.712$	$R^2 = 0.9961$
C	$= -223630x + 14 \times 10^{7x}\, ln(10)$	$R^2 = 0.951$
D	$= -0.6533$	$R^2 = 0.9871$

The rate of change was determined using the formula: $\frac{d}{dx}[x^n] = nx^{n-1}$

Case 3: The analysis of a mixture containing 80% water and 20% ammonia generated four plots A, B, and D, analyzed by linear regression, resulted in a perfect fit for A and strong correlations for B and D, with R-squared values of 1, 0.9961, and 0.9871, respectively. However, in the case of chart C, a second-order polynomial regression was applied, revealing a rate of change described by the equation $y'=-185980x + 14 \times 10^{7x}\, ln(10)$. The R-squared value for chart C is 0.95

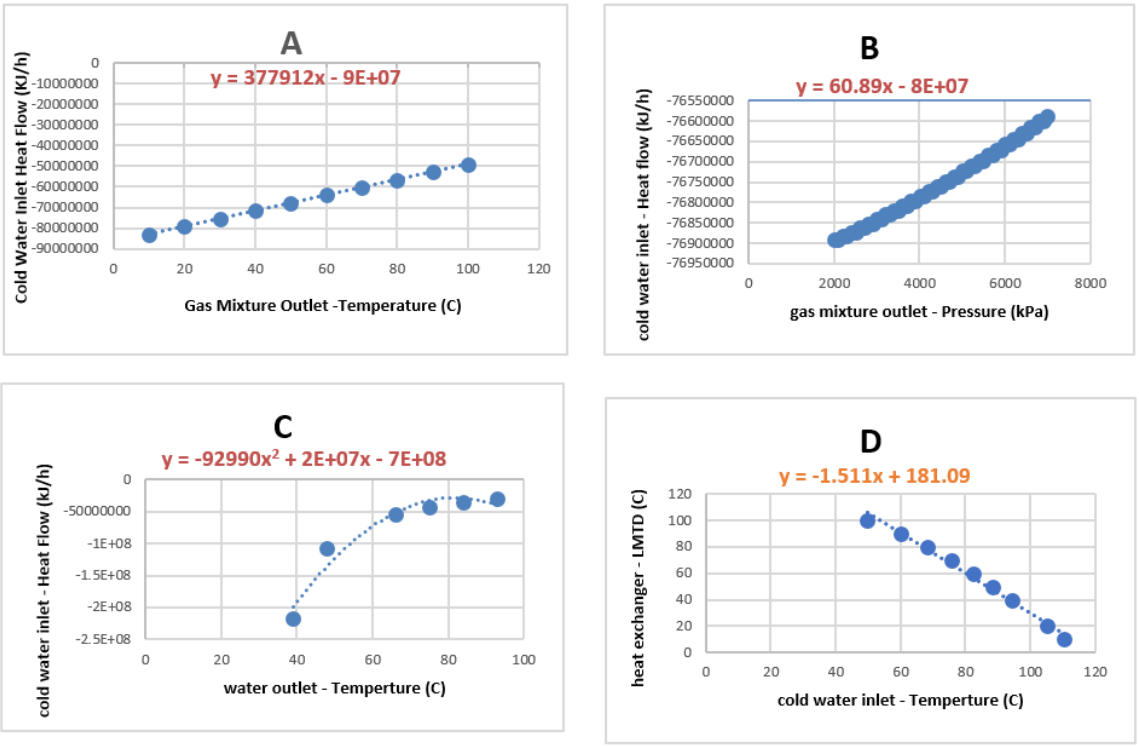

Figure 13: Sensitivity analysis cases at 80% H_2O and 20% NH_3 concentrations in different variables of interest combinations A, B, C, D **(case3).**

Table 6. Values of rate of change and coefficient of determination at 80% water,20% ammonia (**case4).**

Variables of Interest	Rate of Change	R^2 Value
A	$= 377912$	$R^2 = 1$
B	$= 60.89$	$R^2 = 0.9961$
C	$= -185980x + 14 \times 10^{7x}\, ln(10)$	$R^2 = 0.951$
D	$= -1.511$	$R^2 = 0.9871$

The rate of change was determined using the formula: $\frac{d}{dx}\,[x^n] = nx^{n-1}$

Case 4: A fourth case was inducted at conditions of 70% water and 30% ammonia to create four relations with changing different variables. Linear regression was hired to observe the behavior of the plots. Where the results showed a strong correlation for A, B and D, with R-squared values of 1, 0.9961, and 0.9963, respectively. For C, a second-order polynomial regression was applied, revealing a rate of change described by the equation $y'=-173110x + 7 \times 10^{7x}\, ln(10)$. The R-squared value for chart C is 0.951.

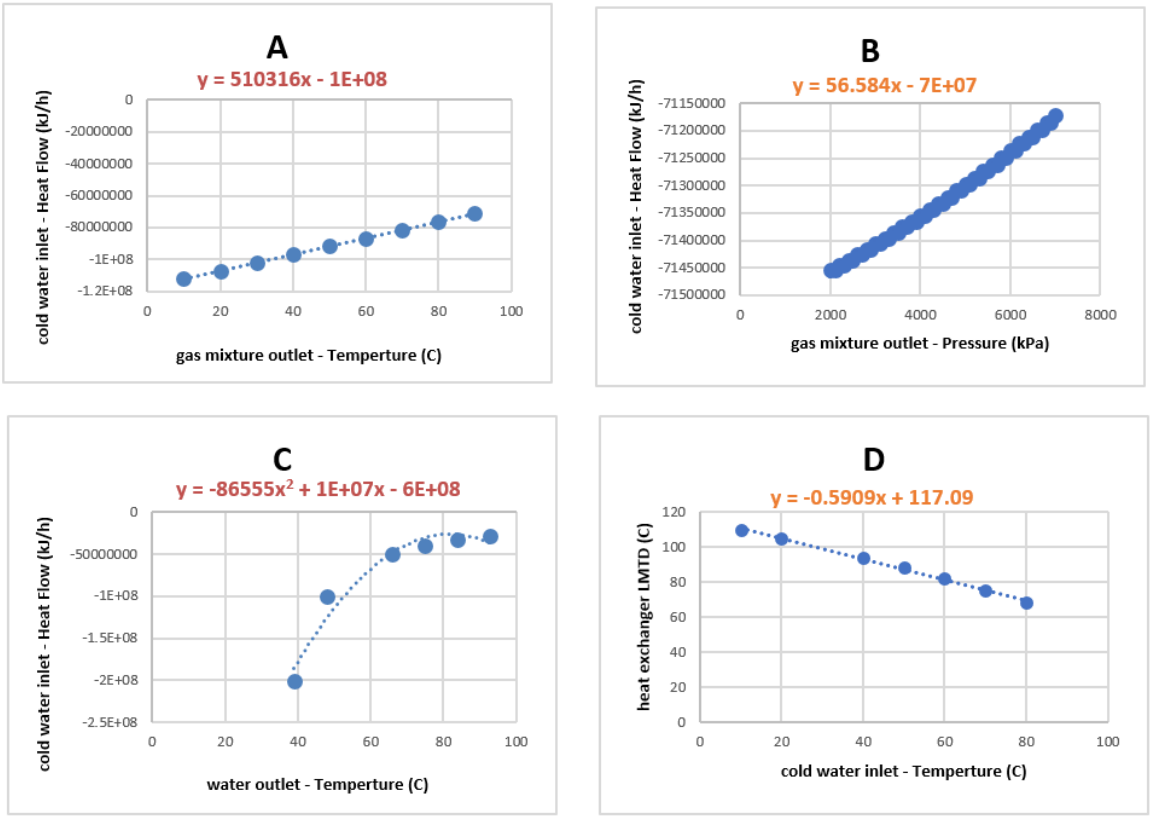

Figure 14: Sensitivity analysis cases at 70% H2O and 30% NH3 concentrations in different variables of interest combinations A, B, C, D **(case 4)**

Table 7. Values of rate of change and coefficient of determination at 70% water,30% ammonia **(case 5).**

Variables of Interest	Rate of Change	R^2 Value
A	$= 510316$	$R^2 = 1$
B	$= 56.58$	$R^2 = 0.9961$
C	$= -173110x + 7 \times 10^{7x}\, ln(10)$	$R^2 = 0.951$
D	$= -0.5909$	$R^2 = 0.9963$

The rate of change was determined using the formula: $\frac{d}{dx}[x^n] = nx^{n-1}$

Case 5: At 60% water and 40% ammonia case, the data analyzed for multiple variables produced four charts. The data were linearly fitted to present R2 values of 1, 0.9961 and 0.9871 for A which showed a perfect fit, B and D. However, a second-order polynomial regression was applied on chart C reporting a rate of change described by the equation $y' = -157924x + 7 \times 10^{7x}\, ln(10)$. The R-squared value for chart C is 0.9493

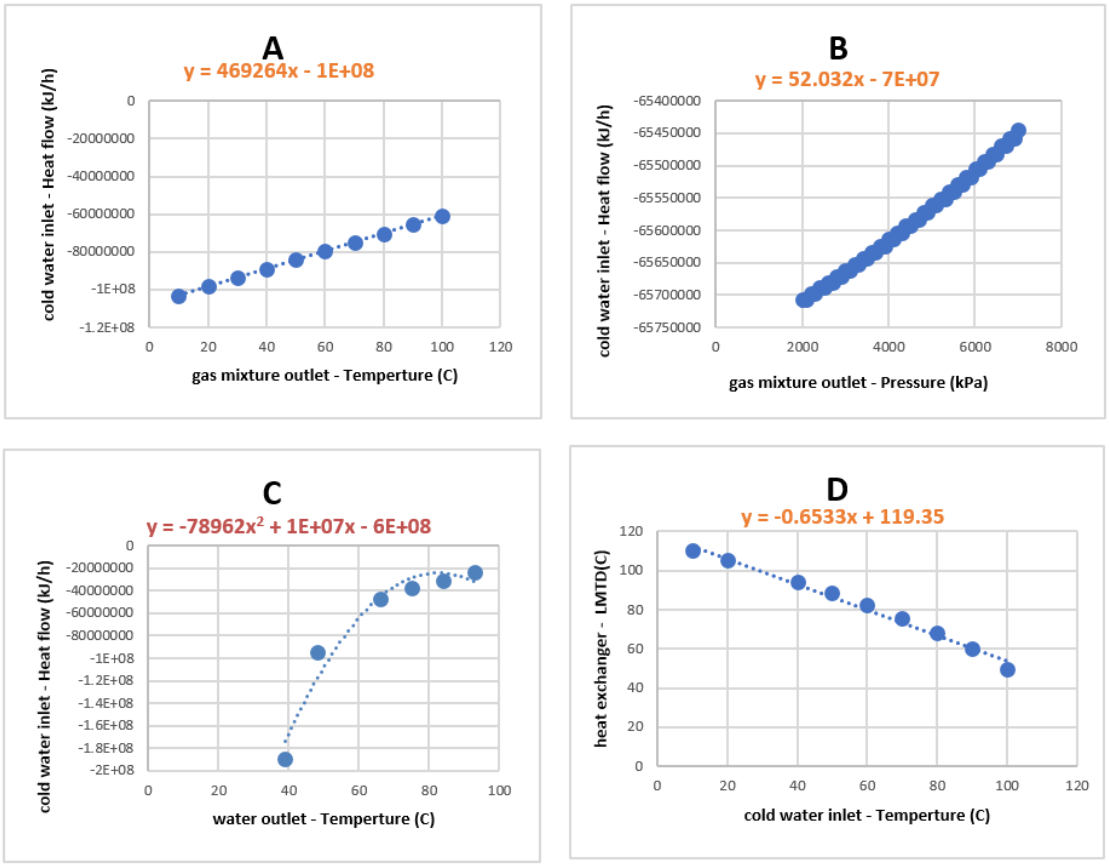

Figure 15: Sensitivity analysis cases at 60% H_2O and 40% NH_3 concentrations in different variables of interest combinations A, B, C, D (case5).

Table 8. Values of rate of change and coefficient of determination at 60% water,40% ammonia (case 5).

Variables of Interest	Rate of Change	R² Value
A	$= 469264$	$R^2 = 1$
B	$= 52.032$	$R^2 = 0.9961$
C	$= -157924x + 7 \times 10^{7x}\, ln(10)$	$R^2 = 0.9493$
D	$= -0.6533$	$R^2 = 0.9871$

The rate of change was determined using the formula: $\frac{d}{dx}[x^n] = nx^{n-1}$

Case 6: A linear trend is observed in Charts (A), (B), and (D), and the fit in (A) is considered ideal with an R-squared value of 1 and a rate of change of 425392, 43.936, and -0.5909, respectively. In the case of (C), there is a noteworthy quadratic relationship with a rate of change described as -140606x + 7 10x ln(10) and an R-squared value of 0.9963.

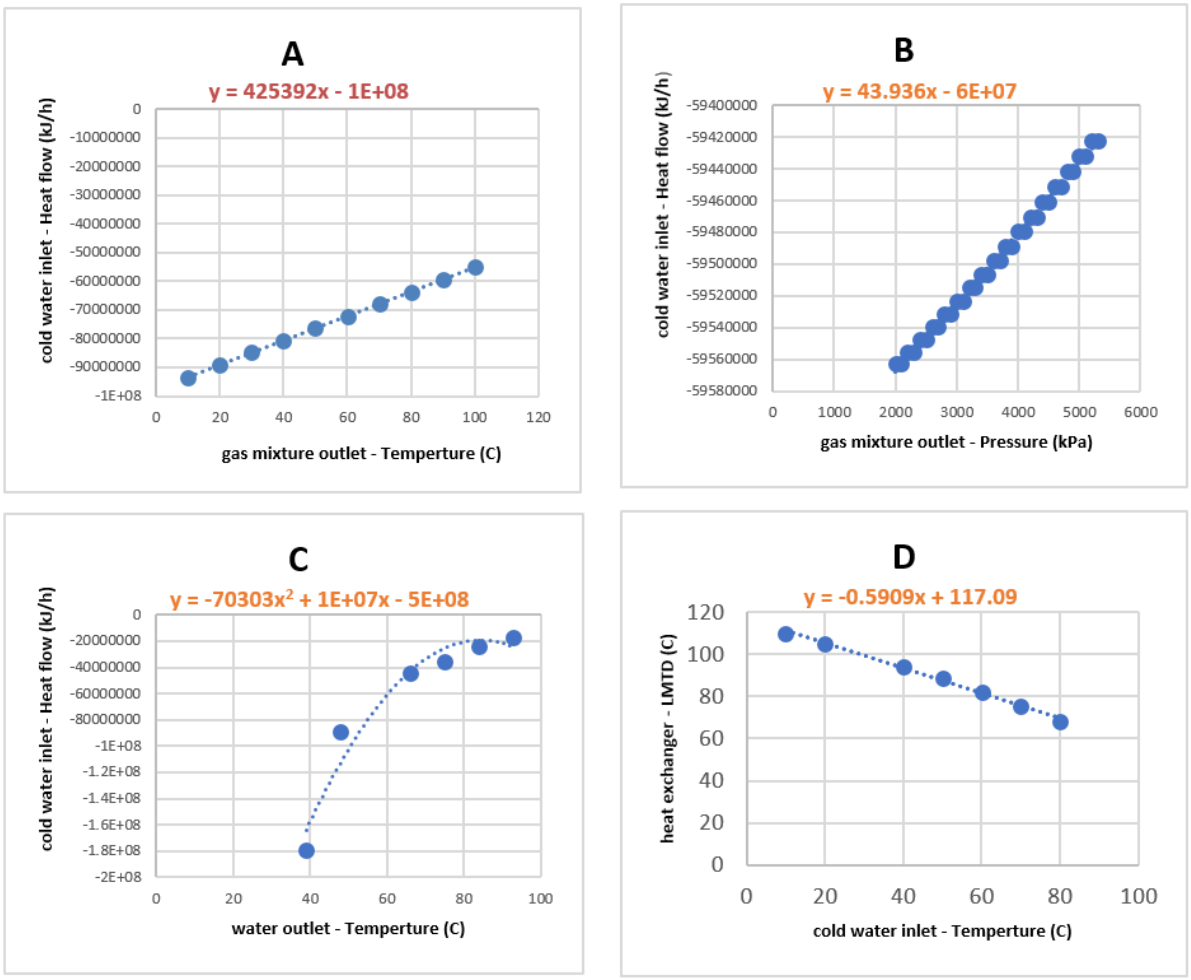

Figure 16: Sensitivity analysis cases at 50% H_2O and 50% NH_3 concentrations in different variables of interest combinations A, B, C, D (case 6).

Table 9. values of rate of change and coefficient of determination at 50% water,50% ammonia (case 6).

Variables of Interest	Rate of Change	R^2 Value
A	$= 425392$	$R^2 = 1$
B	$= 43.936$	$R^2 = 0.996$
C	$= 140606x + 7 \times 10^{7x}\, ln(10)$	$R^2 = 0.9502$
D	$= -0.5909$	$R^2 = 0.9963$

The rate of change was determined using the formula: $\frac{d}{dx}\,[x^n] = nx^{n-1}$

Case 7: The data in charts (A), (B), and (D) are all linearly fitted, with (A) displaying the optimal fit based on the R2 value, which is equal to 1, as indicated in the table. The rates of change for the three graphs presented were 377912, 41.903, and -0.6533. For the case in chart (C), the $R^2 = 0.9587$, and the rate of change is $-136212x + 7 \times 10^{7x}\ln(10)$, demonstrating a strong quadratic relationship between the variables of interest.

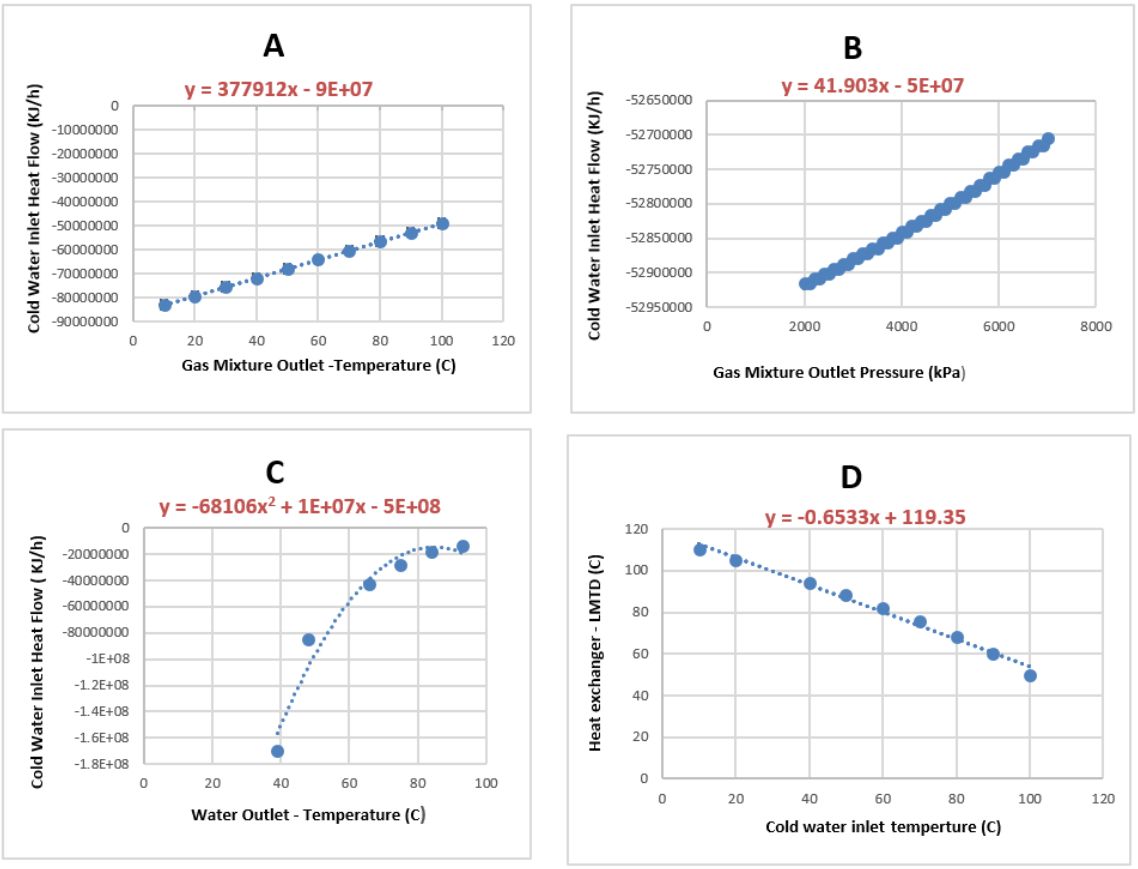

Figure 17: Sensitivity analysis cases at 40% H_2O and 60% NH_3 concentrations in different variables of interest combinations A, B, C, D (case 7).

Table 10. Values of rate of change and coefficient of determination at 40% water,60% ammonia (case 7).

Variables of Interest	Rate of Change	R^2 Value
A	377912	$R^2 = 1$
B	41.903	$R^2 = 0.9961$
C	$-136212x + 7 \times 10^{7x}\ln(10)$	$R^2 = 0.9587$
D	-0.6533	$R^2 = 0.9871$

The rate of change was determined using the formula: $\frac{d}{dx}[x^n] = nx^{n-1}$

Case 8: The data in charts (A), (B), and (D) are all linearly fitted, with (A) displaying the optimal fit based on the R2 value, which is equal to 1, as indicated in the table. The rates of change for the three graphs presented were 377912, 41.903, and -0.6533. For the case in chart (C), the R^2 = 0.9587, and the rate of change $-166480x + 7 \times 10^{7x} ln(10)$, demonstrating a strong quadratic relationship between the variables of interest.

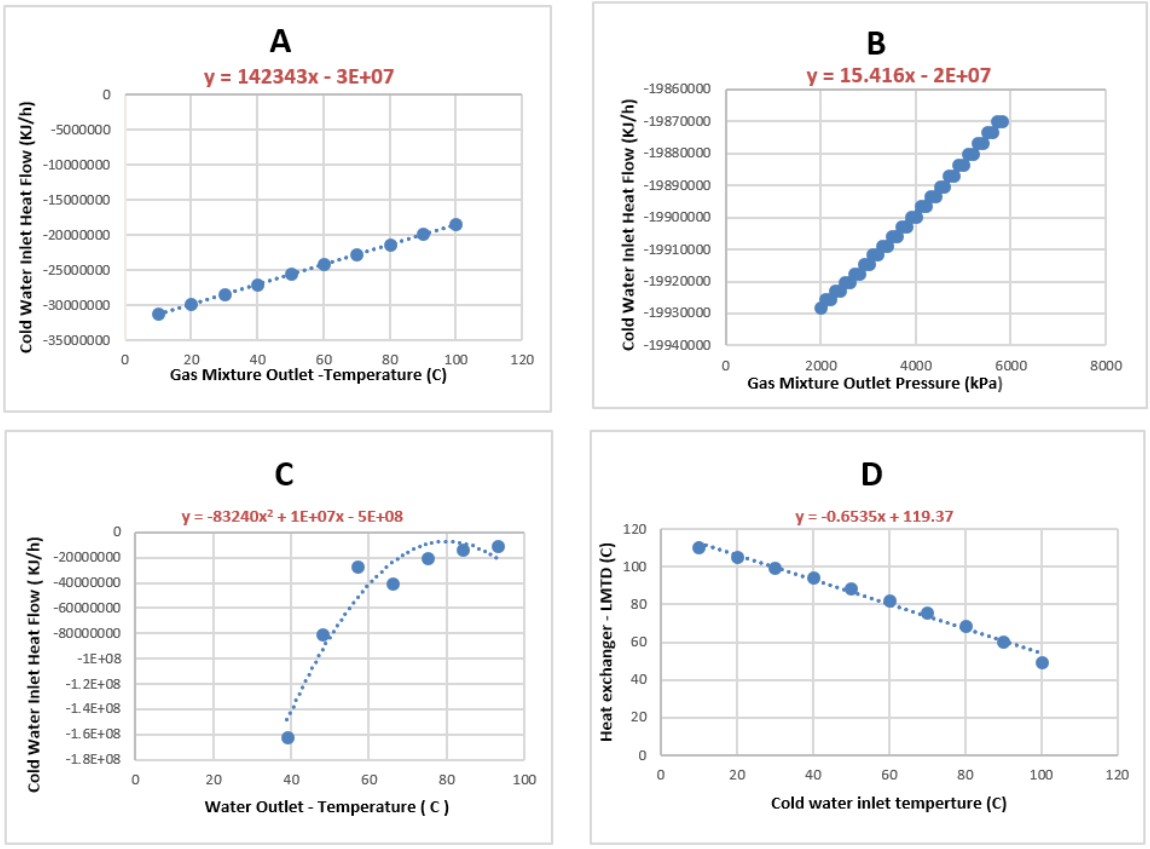

Figure 18: Sensitivity analysis cases at 30% H_2O and 70% NH_3 concentrations in different variables of interest combinations A, B, C, D (case 8).

Table 11. values of rate of change and coefficient of determination at 30% water,70% ammonia (case 8).

Variables of Interest	Rate of Change	R^2 Value
A	142343	R^2 = 1
B	15.416	R^2 = 0.9966
C	$-166480x + 7 \times 10^{7x} ln(10)$	R^2 = 0.9176
D	-0.6535	*R^2 = 0.9882*

The rate of change was determined using the formula: $\frac{d}{dx}[x^n] = nx^{n-1}$

Case 9: The data points in charts (A), (B), and (D) have been fitted into a linear fit, and the correlation between the listed variables of interest was determined to be 6.3032 and -0.6533, respectively, as indicated in Table (13). This presents a perfect fit for (A) and a strong correlation for (B) and (d) with R2 values of R2 = 1, R2 = 0.9963, and R2 = 0.9871. As for the case in (C), it exhibits a polynomial second-order regression with a rate of change of $-191462x + 7 \times 10^{7x} ln(10)$. The R^2 value of 0.8972, suggesting a moderate relationship between water outlet temperature and heat exchanger (LMTD).

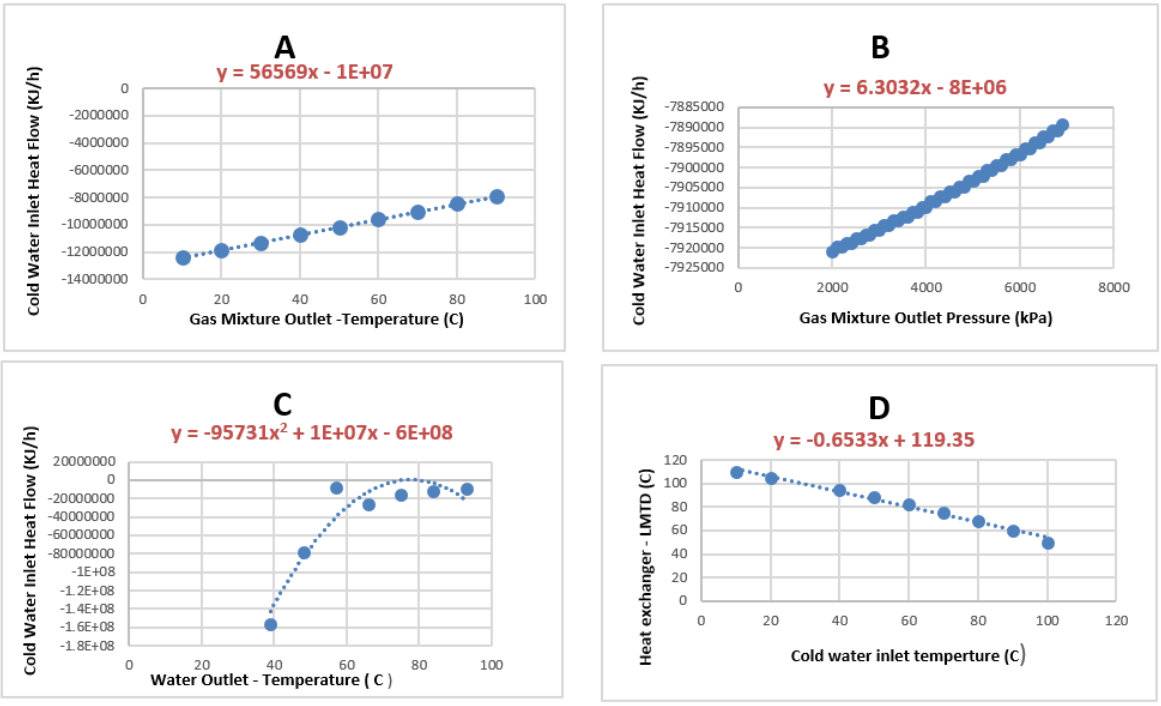

Figure 19: Sensitivity analysis cases at 20% H_2O and 80% NH_3 concentrations in different variables of interest combinations A, B, C, D (case 9).

Table 12. Values of rate of change and coefficient of determination at 20% water,80% ammonia (case 9).

Variables of Interest	Rate of Change	R² Value
A	56569	R² = 1
B	6.3032	R² = 0.9963
C	$-191462x + 7 \times 10^{7x} \ln(10)$	R² = 0.8972
D	−0.6533	R² = 0.9871

The rate of change was determined using the formula: $\frac{d}{dx}[x^n] = nx^{n-1}$

Case 10: charts (A), (B), and (D) of Figure 20 displayed a linear fit with R2 values of 1, 0.9957, and 0.9932, showing an optimal fit for (A) and a significant correlation for both (B) and (D). The rates of change were determined to be as follows: 199290, 21.236, and -0.6169, respectively. In the case of the data in chart (C), quadratic regression has been identified among the variables of interest with a rate of change of $-195038x + 14 \times 10^{7x}\ln(10)$and an R2 value of R2 = 0.951, indicating a notable association.

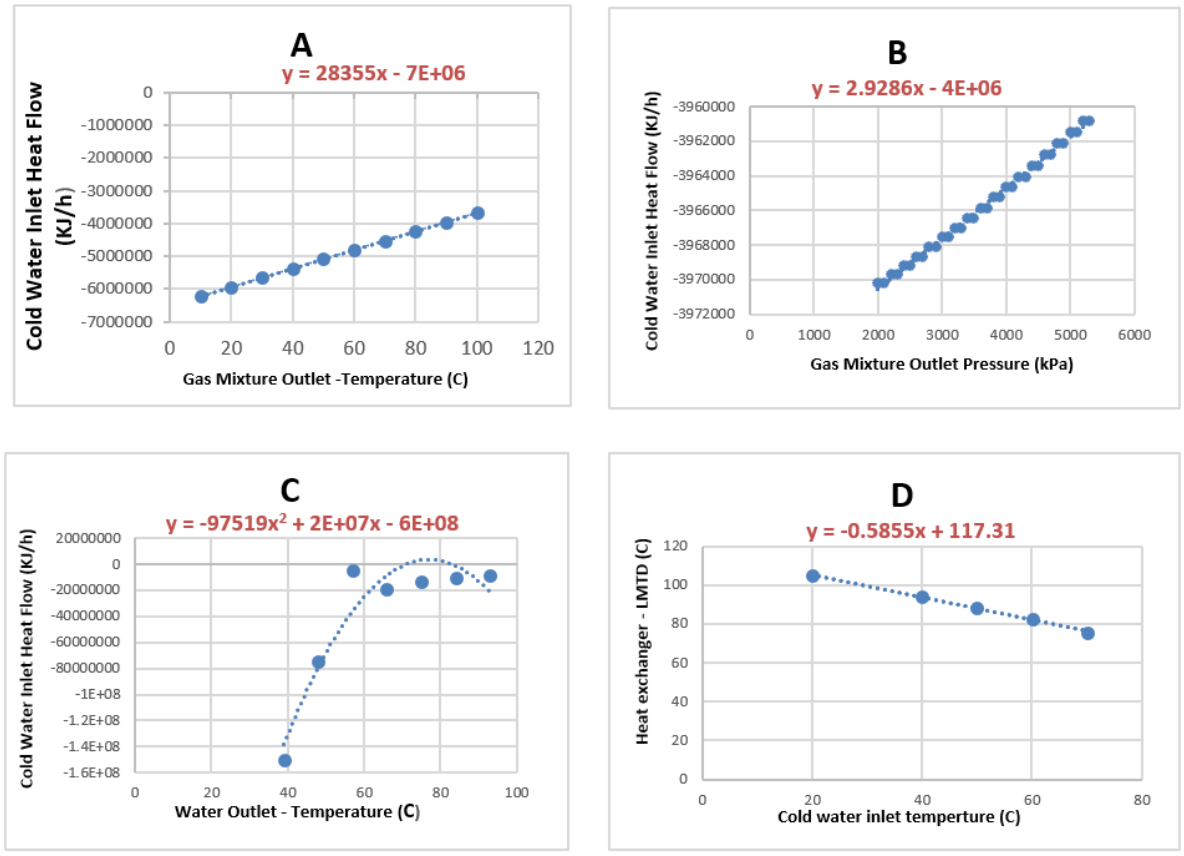

Figure 20: Sensitivity analysis cases at 10% H2O and 90% NH3 concentrations in different variables of interest combinations **A, B, C, D (case 10).**

Table 13. Values of rate of change and coefficient of determination at 10% water,90% ammonia **(case 10)**.

Variables of Interest	Rate of Change	R² Value
A	28355	R² = 1
B	2.9286	R² = 0.996
C	$-195038x + 14 \times 10^{7x}\ln(10)$	R² = 0.8987
D	-0.5855	R² = 0.9979

The rate of change was determined using the formula: $\frac{d}{dx}[x^n] = nx^{n-1}$

Case 11: A Linear correlation has been demonstrated among the variables of interest in the data set presented in plots (A), (B), and (D) with rates of change of 28355, 2.9286.-0.58556, respectively. Furthermore, plot (A) shows a very high correlation with R2 = 1, while plots (B) and (d) indicate a significant correlation with R2 values of R2 = 0.996 and R2 = 0.9979. In chart (C), a second order quadratic regression with a rate of change of $-71458\ x + 36\times10^{6x}\ \ln(10)$ is shown. Given a R value of 0.8987.

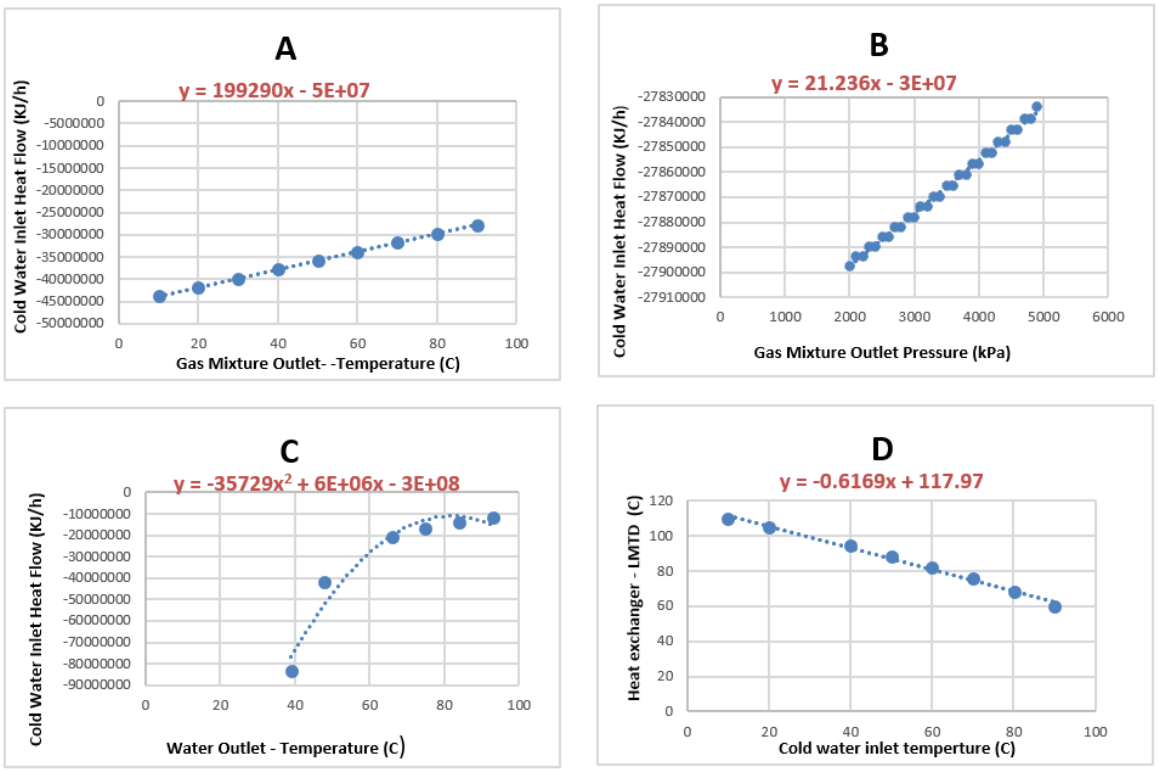

Figure 21: Sensitivity analysis cases at 0% H_2O and 100% NH_3 concentrations in different variables of interest combinations A, B, C, D (case 11).

Table 14. Values of rate of change and coefficient of determination at 0% water,100% ammonia (case 11).

Variables of Interest	Rate of Change	R² Value
A	199290	R² = 1
B	21.236	R² = 0.9957
C	$-71458\ x + 36\times10^{6x}\ \ln(10)$	R² = 0.951
D	-0.6169	R² = 0.9932

The rate of change was determined using the formula: $\frac{d}{dx}\ [x^n] = nx^{n-1}$

Conclusion

The investigation conducted by the research team involved the analysis of two heat-exchanging systems. Specifically, the shell and tube model were analyzed, and various NH_3-H_2O concentrations were explored using the ASPEN analytic tool. Regarding the second system, the helical heat exchanger design exhibited enhanced effectiveness in fluid cooling due to its structural and geometrical attributes. However, it is essential to acknowledge that integrating ammonia into the cooling system requires a thorough assessment of various factors and aspects related to ammonia. These include safety regulations, environmental considerations, health impacts, sustainability, and financial implications. These factors are crucial in determining the feasibility and suitability of using ammonia as a cooling agent in the heat exchanger. Therefore, future research should prioritize the evaluation of these criteria.

Abbreviations

SMR	Steam-Methane-Reforming
HP	High-Temperature
BWF	Boiler Water Feed
HB	Haber-Bosch
HTS	High-Temperature-Shift
LTS	Low-Temperature-Shift
WGS	Water Gas Shif
MDEA	methyldiethanolamine
MEA	Monoethanolamine
SRKC	Steam Rankine Cycle
POX	Partial oxidation
SYN	Synthesis
ATR	Autothermal Reformer
MTS	Medium-Temperature-Shift
PSA	Pressure swing adsorption
TKIS	ThyssenKrupp Industrial Solutions
AWE	Alkaline-water-electrolysis
ASU	Air Separation Unit
SNG	Syngas
KBR	Kellogg Brown & Root
MWK	M.W. Kellogg
ICI	Imperial Chemical Industries
KRES	KBR Reforming Exchanger System
KAAP	KBR Advanced Ammonia Processing
MTPD	Metric Tons Per Day
LAC	Linde-Ammonia-Concep
FTR	Fired Tubular Reformer
i-WGS	isothermal water gas shift
IP	Intermediate pressure

References

[1] Cheremisinoff NP, Rosenfeld PE, editors. Industry and Products. Handb. Pollut. Prev. Clean. Prod. Best Pract. Agrochem. Ind., Elsevier; 2011, p. 1–24. doi: 10.1016/b978-1-4377-7825-0.00001-7.

[2] Aalrebei, Odi Fawwaz, Anwar Hamdan Al Assaf, Abdulkarem Amhamed, Nedunchezhian Swaminathan, and Sally Hewlett. "Ammonia-hydrogen-air gas turbine cycle and control analyses." International Journal of Hydrogen Energy 47, no. 13 (2022): 8603-8620.

[3] van Rooij A. Engineering contractors in the chemical industry. the development of ammonia processes, 1910–1940. HistTechnol 2005;21:345–66. doi:10.1080/ 07341510500 268215.

[4] Tso WW, DogaDemirhan C, Powell JB, Pistikopoulos EN. Toward Optimal Synthesis of Renewable Ammonia and Methanol Processes (RAMP). Comput. Aided Chem. Eng., vol. 44, Elsevier B.V.; 2018, p. 1705–10. doi:10.1016/B978-0- 444-64241-7.50279-2.

[5] Pearson A. Refrigeration with ammonia. Int J Refrig 2008;31(4):545–51. https:// doi.org/10.1016/ j.ijrefrig. 2007. 11.011.

[6] Kusmanov SA, Smirnov AA, Kusmanova YV, Belkin PN. Anode plasma electrolytic nitrohardening of medium carbon steel. Surf Coatings Technol 2015;269:308–13. https://doi.org/10.1016/ j.surfcoat.2014.12.033.

[7] Kristiana I, Lethorn A, Joll C, Heitz A. To add or not to add: The use of quenching agents for the analysis of disinfection byproducts in water samples. Water Res 2014;59:90–8. https://doi.org/10.1016/j.watres.2014.04.006.

[8] Brightling John. Ammonia and the fertiliser industry: the development of ammonia at Billingham. Johnson Matthey Technol Rev 2018;62(1):32–47. https://doi.org/10.1595/ 205651318X696341.

[9] Rafiqul Islam, Weber Christoph, Lehmann Bianca, Voss Alfred. Energy efficiency improvements in ammonia production—perspectives and uncertainties. Energy 2005;30(13):2487–504. https://doi.org/10.1016/j.energy.2004.12.004.

[10] ChehadeGhassan, Dincer Ibrahim. Development and analysis of a polygenerational smart energy hub for sustainable communities. Energy Convers Manag 2020;226:113475. https://doi.org/10.1016/j.enconman.2020.113475.

[11] Malinowski, Z., John G. Lenard, and M. E. Davies. "A study of the heat-transfer coefficient as a function of temperature and pressure." Journal of materials processing technology 41, no. 2 (1994): 125-142.

[12] de Roode, S.R., et al., A diagnosis of excessive mixing in smagorinsky subfilter-scale turbulent kinetic energy models. Journal of the Atmospheric Sciences, 2017. 74(5): p. 1495-1511.

[13] Dimotakis, P.E., Turbulent mixing. Annual Review of Fluid Mechanics, 2005. 37: p. 329-356.

[14] Lee, S. and P. Harsha, Use of turbulent kinetic energy in free mixing studies. AIAA Journal, 1970. 8(6): p. 1026-1032.

[15] Uwem Ekere lnyang and Iniubong James Uwa (2022) Heat transfer in Helical coil Heat Exchanger, *Advances in Chemical Engineering and science*, 12(1)

[16] Alrebei, Odi Fawwaz, Abdulkarem I. Amhamed, Muftah H. El-Naas, Mahmoud Hayajnh, Yasmeen A. Orabi, Ward Fawaz, Ahmad S. Al-tawaha, and Agustin Valera Medina. "State of the art in separation processes for alternative working fluids in clean and efficient power generation." Separations 9, no. 1 (2022): 14.

[17] Alrebei, Odi Fawwaz, Anwar Hamdan Al Assaf, Mohammad S. Al-Kuwari, and Abdulkarem Amhamed. "Lightweight methane-air gas turbine controller and simulator." Energy Conversion and Management: X 15 (2022): 100242.

[18] Amhamed, Abdulkarem I., Syed Shuibul Qarnain, Sally Hewlett, Ahmed Sodiq, Yasser Abdellatif, Rima J. Isaifan, and Odi Fawwaz Alrebei. "Ammonia production plants—A review." Fuels 3, no. 3 (2022): 408-435.

[19] Alrebei, Odi Fawwaz, Laurent M. Le Page, Sally Hewlett, Yusuf Bicer, and Abdulkarem Amhamed. "Numerical investigation of a first-stage stator turbine blade subjected to NH3–H2/air combustion flue gases." International Journal of Hydrogen Energy 47, no. 78 (2022): 33479-33497.

[20] Hamdan Al Assaf, Anwar, Abdulkarem Amhamed, and Odi Fawwaz Alrebei. "State of the Art in Humidified Gas Turbine Configurations." Energies 15, no. 24 (2022): 9527.

[21] Alrebei, Odi Fawwaz, Laurent M. Le Page, Gordon Mckay, Muftah H. El-Naas, and Abdulkarem I. Amhamed. "Recalibration of carbon-free NH3/H2 fuel blend process: Qatar's
roadmap for blue ammonia." International Journal of Hydrogen Energy (2023).

[22] Rashid, Farhan & Talib, Shahidmahdy & Hussein, Ahmed & Taha, Obai. "An Experimental Investigation of Double Pipe Heat Exchanger Performance and Exergy Analysis Using Air Bubble Injection Technique." Jordan Journal of Mechanical and Industrial Engineering (2022), Vol. 16, no. 2. p. 195 - 204.

[23] Al-Maghalseh, Maher. "Investigate the natural convection heat transfer in a PCM thermal storage system using ANSYS/FLUENT." Jordan Journal of Mechanical and Industrial Engineering (2017), vol. 11, no. 4, p. 217-223.

[24] Aboushi, Ahmad. (2016). "Solar Thermal Hybrid Heating System." Jordan Journal of Mechanical and Industrial Engineering (2016), vol. 11, no. 3, p. 181-184.

[25] Kalaivanan, R. & Rathnasamy, R. "Experimental investigation of forced convective heat transfer in rectangular micro-channels." Jordan Journal of Mechanical and Industrial Engineering (2011), vol 5, no. 5, p 383-387.

[26] Beithou, N. & Abu-Hilal, Mohammed. "Hot Water Management of DHW Storage Tank: Supply Features." Jordan Journal of Mechanical and Industrial Engineering (2022), vol. 4, no. 6, p. 789 - 796.

[27] Hossain, R. & Chowdhuri, Mohammad & Feroz, C. "Design, Fabrication and Experimental Study of Heat Transfer Characteristics of a Micro Heat Pipe." Jordan Journal of Mechanical and Industrial Engineering (2010), vol. 4, no. 5, p. 531 - 542.

[28] Gomri, Rabah. "Seawater Desalination System Integrated to Single Effect and Double Effect Absorption Heat Transformers." Jordan Journal of Mechanical and Industrial Engineering (2010), vol. 4, no. 1, p. 217 - 224.

[29] Ali, A. & AL-Soud, Mohammed & Abdallah, Essam & Addallah, Salah. "Water Pumping System with PLC and Frequency Control." Jordan Journal of Mechanical and Industrial Engineering (2009), vol. 3, no. 3, p. 216 - 221.

[30] Ganesh Murali J., Subrahmanya S. Katte. "Experimental Investigation of Heat Transfer Enhancement in Radiating Pin Fin." Jordan Journal of Mechanical and Industrial Engineering (2008), vol. 2, no. 3, p. 163 - 167.